ANTIOXIDANTS & REDOX SIGNALING
Volume 10, Number 3, 2008

DOI: 10.1089/ars.2007.1792

Original Research Communication

Regulation of Proliferation of Skeletal Muscle Precursor Cells by NADPH Oxidase

MAHROO MOFARRAHI,[1] RALF P. BRANDES,[2] AGNES GORLACH,[3] JOERG HANZE,[4] LANCE S. TERADA,[5] MARK T. QUINN,[6] DOMINIQUE MAYAKI,[1] BASIL PETROF,[1] and SABAH N.A. HUSSAIN[1]

ABSTRACT

Skeletal muscle precursor cells are adult stem cells located among muscle fibers. Proliferation, migration, and subsequent differentiation of these cells are critical steps in the repair of muscle injury. We document in this study the roles and mechanisms through which the NAPDH oxidase complex regulates muscle precursor cell proliferation. The NADPH oxidase subunits Nox2, Nox4, $p22^{phox}$, $p47^{phox}$, and $p67^{phox}$ were detected in primary human and murine skeletal muscle precursor cells. In human muscle precursor cells, NADPH oxidase-fusion proteins were localized in the cytosolic and membrane compartments of the cell, except for $p47^{phox}$, which was detected in the nucleus. In proliferating subconfluent precursor cells, both Nox2 and Nox4 contributed to O_2^- production. However, Nox4 expression was significantly attenuated in differentiated myotubes. Proliferation of precursor cells was significantly reduced by antioxidants (*N*-acetylcysteine and apocynin), inhibition of $p22^{phox}$ expression by using siRNA oligonucleotides, and reduction of Nox4 and $p47^{phox}$ activities with dominant-negative vectors and siRNA oligonucleotides resulted in attenuation of activities of the Erk1/2, PI-3 kinase/AKT and NFκB pathways and significant reduction in cyclin D1 levels. We conclude that NADPH oxidase is expressed in skeletal muscle precursor cells and that its activity plays an important role in promoting proliferation of these cells. *Antioxid. Redox Signal.* 10, 559–574.

INTRODUCTION

It has been well established that relatively low levels of reactive oxygen species (ROS) play important roles as signaling molecules in a wide range of physiologic and pathophysiologic responses. However, excessive production of ROS leads to cell injury and apoptosis and is involved in the pathogenesis of many diseases, including diabetes, hypertension, and atherosclerosis (9). ROS are primarily generated as byproducts of mitochondrial oxidative phosphorylation, with O_2^- as the main product. Endoplasmic reticulum cytochrome P-450 enzymes, xanthine, and aldehyde oxidases, nuclear electron-transport systems, flavoproteins, and lipooxygenases are also capable of producing ROS.

In phagocytes, NADPH oxidase is a multimeric enzyme complex consisting of four essential subunits ($p22^{phox}$, $gp91^{phox}$ (Nox2), $p47^{phox}$ and $p67^{phox}$) and two additional subunits ($p40^{phox}$ and Rac2). $p22^{phox}$ and Nox2 form an integral membrane-bound complex (flavocytochrome b_{558}) that is responsible for catalytic activity, whereas $p47^{phox}$ and $p67^{phox}$ are normally localized in the cytosol (2). On phagocyte stimulation, activation of Rac2 and phosphorylation of $p47^{phox}$ triggers as-

[1]Critical Care, Respiratory and Molecular Endocrinology Divisions, Department of Medicine, McGill University Health Centre, Montréal, Québec, Canada.
[2]Institut fur Kardiovaskulare Physiologie, Fachbereich Medizin der J.W. Goethe-Universitat, Frankfurt am Main, Germany.
[3]Experimental Pediatric Cardiology, Department of Pediatric Cardiology and Congenital Heart Disease, German Heart Center Munich at the TU Munich, Munich, Germany.
[4]Department of Internal Medicine, Medical School, University of Giessen, Giessen, Germany.
[5]Department of Medicine, University of Texas Southwestern Medical Center, Dallas, Texas.
[6]Department of Veterinary Molecular Biology, Montana State University, Bozeman, Montana.

sembly of $p47^{phox}$ and $p67^{phox}$ subunits with $p40^{phox}$ and Rac2, as well as translocation of these subunits to flavocytochrome b_{558}, leading eventually to the formation of a functional NADPH oxidase complex.

Recent studies have indicated that NADPH oxidase is also a major source of ROS in nonphagocytes, including vascular and airway smooth muscles, fibroblasts, and endothelial and epithelial cells [for review, see (4)]. In these cells, NADPH oxidase produces ROS under basal conditions, but, on stimulation, ROS are produced intracellularly at much lower levels than they are in phagocytes. Another difference between phagocytes and nonphagocytes relates to the fact that several homologues of Nox2 (including Nox1, Nox3, Nox4, and Nox5), and of $p47^{phox}$ (NOXO1) and $p67^{phox}$ (NOXOA1), are expressed in various nonphagocytic cells, indicating that multiple NADPH oxidase forms might exist in these cells (3, 10). In addition, increasing evidence indicates that in nonphagocytes, Nox-derived ROS function as second messengers in the signaling of tyrosine kinase growth factor receptors, cytokine receptors, and G protein–coupled receptors, such as those associated with angiotensin II (4).

Skeletal muscles have a relatively high regenerative capacity because of the presence of satellite (muscle precursor) cells, which are mononuclear progenitor cells located between the basal lamina and cell membranes of mature muscle fibers. Under normal conditions, satellite cells are quiescent. However, in response to muscle injury or during degenerative muscle diseases, precursor cells are activated and go through rounds of cell division to produce a pool of myogenic precursors known as myoblasts. A number of these myoblasts replenish satellite cell reserves, but the majority proliferate further, fuse, and finally differentiate into multinucleated myotubes and, eventually, myofibers (19).

Little information is available regarding the expression and functional significance of NADPH oxidase–derived ROS in skeletal muscle precursor cells. Two recent studies have confirmed the presence of Nox2, $p47^{phox}$, and $p67^{phox}$ mRNA and proteins in immortalized rat L6 myoblasts and myotubes and that the activity of NADPH oxidase in these cells generates ROS to regulate insulin signaling and Ca^{2+} flux (12, 41). Others, however, have failed to detect NADPH oxidase expression in either immortalized mouse C2C12 or L6 myoblasts (21). The reasons behind these discrepancies are unclear, but may be related to methodologic issues, including differences in the type of immortalized precursor cells under investigation.

TABLE 1. LIST OF OLIGONUCLEOTIDES PRIMERS USED FOR RT-PCR AND REAL-TIME PCR AMPLIFICATION OF NADPH OXIDASE SUBUNITS AND NOX PROTEINS IN HUMAN AND MURINE SKELETAL MYOBLASTS AND MYOTUBES

Target	*Product size bp*	*Sequences*	*Reference*	*Species*
$p22^{phox}$	164	Forward-GTACTTTGGTGCCTACTCCA Reverse-CGGCCCGAACATAGTAATTC	(1)	H*
$p22^{phox}$	176	Forward-TCTATCGCTGCAGGTGTGCT Reverse-AGGCACCGACAACAGGAAGT		M*
Nox1	281	Forward-CTTCCTCACCGGATGGGACA Reverse-TGACAGCATTTGCGCAGGCT	(1)	M&H
Nox2	321	Forward-TGTCCAAGCTGGAGTGGCAC Reverse-GCACAGCCAGTAGAAGTAGAT	(1)	H
Nox2	156	Forward-CCAGTGAAGATGTGTTCAGCT Reverse-GCACAGCCAGTAGAAGTAGAT		H*
Nox3	708	Forward-GAGTGGCACCCCTTCACCCT Reverse-CTAGAAGCTCTCCTTGTTGT	(1)	H
Nox4	1741	Forward-GCCGCCGCCATGGCTGTGTCCTGG Reverse-GGCATAACACAGCTGATTGATTCCGCTGAG	(13)	H
Nox4	211	Forward-AGTCAAACAGATGGGATA Reverse-TGTCCCATATGAGTTGTT	(1)	M&H
Nox4	285	Forward-TTGTCTTCTACATGCTGCTG Reverse-AGGCACAAAGGTCCGHAAAT		M&H*
Nox4	240	Forward-AAGCATACTTGCCCCAGCTG Reverse-CAGGCCAATGGCCTTCATGT	(1)	M&H
$p47^{phox}$	207	Forward-TTGAGAAGCGCTTCGTACCC Reverse-CGTCAAACCACTTGGGAGCT	(1)	H
$p47^{phox}$	93	Forward-CCCAGCCAGCACTATGTGTA Reverse-GGAACTCGTAGATCTCGGTG		M&H*
$p67^{phox}$	245	Forward-CAGTTCAAGCTGTTTGCCTG Reverse-TTCTTGGCCAGCTG	(1)	M&H*
CyclophilinB	265	Forward-ATGGCACAGGAGGAAAGAGC Reverse-ATGATCACATCCTTCAGGGG	(1)	M&H
GADPH	166	Forward-AAGAAGGTGGTGAAGCAGGCG Reverse-ACCAGGAAATGAGCTTGACAA		M&H*

*Primers used for Real-time PCR.

In our attempts to evaluate the expression, intracellular localization, and functional importance of various subunits of NADPH oxidase enzyme complex in skeletal precursor cells, we performed several pilot experiments in which we used cultured primary human and murine muscle precursor cells. Based on these preliminary results and the well-documented involvement of Nox proteins in the regulation of proliferation of several nonphagocytic cell types, we tested in this study the following hypotheses: (a) The NAPDH oxidase enzyme complex is present in mature skeletal muscle fibers and skeletal muscle precursor cells; (b) both Nox2 and Nox4 contribute to total NAPDH oxidase activity in proliferating primary skeletal muscle precursor cells; (c) NADPH oxidase–derived ROS promote proliferation of muscle precursor cells by activating the Erk1/2, PI-3 kinase/AKT, and the NF-κB pathways.

MATERIALS AND METHODS

Animal preparation

Six-week-old male C57/BL6 mice were killed with an overdose of pentobarbital sodium. Diaphragm, extensor digitorum longus (EDL), tibialis anterior, and soleus muscles were immediately excised, frozen in liquid nitrogen, and stored at −80°C until further analysis.

Cell culture

Primary human myoblast culture. Primary human muscle precursor cells (human myoblasts), immortalized by expression of the E6E7 early region from human papillomavirus type 16, were generously provided by Dr. E. Shoubridge (McGill University, Montréal, QC) and cultured in SkBM culture medium (SkBM Bullet Kit; Cambrex, East Rutherford, NJ), supplemented with 15% inactivated fetal bovine serum (FBS) (28). To induce differentiation into myotubes, myoblasts (90% confluent) were grown in Dulbecco's modified Eagle's medium (DMEM) (Invitrogen Inc., Carlsbad, CA) supplemented with 2% inactivated horse serum (HS) for 6 days. Differentiation was evaluated, with immunoblotting, by the morphologic appearance of cells and by measuring the expression of myogenin and muscle-specific proteins, including myosin heavy chain and creatine kinase.

Primary murine myoblast culture. Primary murine muscle precursor cells (mouse myoblasts) derived from diaphragm and tibialis anterior muscles were established as described by Rosenblatt *et al.* (33). In brief, diaphragm and tibialis anterior muscle strips were extracted from 6-week-old C57/BL6 mice, digested with collagenase (0.2% at 37°C for 60 min), and then triturated to break muscle tissues into single fibers. Individual fibers were washed in DMEM and phosphate-buffered saline, transferred into matrigel-coated (1 mg/ml in DMEM) six-well plates, and maintained in DMEM supplemented with 1% penicillin/streptomycin and 0.2% amphotericin B, 10% HS, and 0.5% chick embryo extract (MP Biomedicals, Aurora, OH) for 4 days, which allowed myoblasts to attach to the substratum. Myoblasts were then grown in growth medium (DMEM supplemented with 20% fetal bovine serum, 10% HS, 1% chick embryo extract) for 6 days. We should emphasize that this method of myoblast isolation yields >95% pure muscle myoblast population. Identical growth medium was used to maintain immortalized murine C2C12 cells. Total RNA was extracted from primary human and murine as well as C2C12 myoblasts.

Reverse transcriptase-PCR (RT-PCR) and real-time PCR

Total RNA from mouse diaphragm, EDL, tibialis anterior, and soleus muscles and mouse and human myoblasts and myotubes was extracted by using a GenElute Mammalian Total RNA Miniprep Kit (Sigma-Aldrich Co., Oakville, ON, Canada). Total RNA (2 μg) was reverse transcribed by using 200 Superscript II Reverse Transcriptase (Invitrogen) in a reaction mixture containing 0.5 m*M* dATP, dCTP, dGTP, and dTTP, 40 units of RNase inhibitor, 50 pmol random hexamers, 3 m*M* $MgCl_2$, 75 m*M* KCl, 50 m*M* Tris-HCl (pH 8.3), and DTT 20 m*M* in a total volume of 20 μl. The resultant cDNA was PCR amplified by using TaqDNA polymerase (Invitrogen) and oligonucleotide primers specific for murine and human $p22^{phox}$, $p47^{phox}$, $p67^{phox}$, Nox1-Nox5, and cyclophilin B transcripts (control) (Table 1). For all genes, except Nox4, the amplification cycles consisted of initial denaturation at 94°C for 3 min followed by 35 cycles of 30 sec at 94°C, 30 sec at 57°C, and 30 sec at 72°C. For Nox4, the annealing temperature was 50°C. RT- PCR products were analyzed on a 2% agarose gel.

Real-time PCR was performed by using a 7500 Real-Time PCR System (Applied Biosystems, Foster City, CA) and primers designed to amplify human and mouse transcripts of Nox2, Nox4, $p22^{phox}$, $p47^{phox}$, $p67^{phox}$, and GAPDH (see Table 1). One microliter of the reverse-transcriptase reaction was added to 25 μl of SYBR Green PCR Master Mix (Qiagen Inc., Valencia, CA) and 3.5 μl of each 10 μM primer. The thermal profile was as follows: 95°C for 10 min and 40 cycles of 95°C for 15 sec, 57°C for 30 sec, and 72°C for 33 sec. A melt analysis for each PCR experiment was used to assess primer-dimer formation or contamination. Results were analyzed by using the comparative threshold cycle (C_T), the value at which the amplification curve crosses the threshold line. C_T values were then used to calculate absolute copy numbers based on standard curves generated by plasmids containing full-length coding sequences of NADPH oxidase subunits. All real-time PCR experiments were performed in triplicate.

Measurements of O_2^- production

Production of O_2^- in muscle precursor cells was measured by using lucigenin and coelenterazine chemiluminescence assays in 96-well plates with an LMax II luminometer (Molecular Devices Corp., Sunnyvale, CA). In brief, 70% confluent myoblasts or myotubes were washed with PBS and scraped off the plate into cold HBSS buffer. Cells (50×10^4) were loaded in each well of a 96-well plate. NADH or NADPH (100 μM) and lucigenin (10 μM) or coelenterazine (10 μM) were added to each well, and luminometer output (relative light unit) was measured for a 20-min period. Production of O_2^- (total signal minus background signal) was measured as the area under the

TABLE 2. EXPRESSION OF mRNA OF NADPH OXIDASE SUBUNITS IN MOUSE SKELETAL MUSCLES EXPRESSED IN COPIES/ng TOTAL RNA

	Gp91^{phox}/Nox2	*p22^{phox}*	*p47^{phox}*	*p67^{phox}*	*Nox4*
Diaphragm	61 ± 18†	314 ± 12	33 ± 5†	14 ± 3†	27 ± 3†
Extensor digitorium longus	1.6 ± 0.7*†	17 ± 10*	2.4 ± 0.8*†	0.1 ± 0.7*†	1.1 ± 0.2*†
Tibialis anterior	10 ± 2*†	162 ± 14*	9 ± 4*†	2.2 ± 0.4*†	5.1 ± 0.3*†
Soleus	7.0 ± 0.8*†	233 ± 15*	8 ± 2*†	5.2 ± 1.2*†	4 ± 0.8*†

Values are means (six independent samples) ± SEM.
*$p < 0.05$ compared with the diagphragm (using two-way ANOVA).
$^{\dagger}p < 0.05$ compared with p22^{phox}.

curve. In a few experiments, polyethylene glycol superoxide dismutase (PEG-SOD) (250 U/ml), N-acetylcysteine (NAC, 10 m*M*), which is a general antioxidant, apocynin (1 m*M*), which is an inhibitor of the association of p47^{phox} with p22^{phox} and Nox2, and diphenyleneiodonium (DPI, 10 μM), which is an inhibitor of electron transporters, were added 1 h before the addition of NADPH and lucigenin. To evaluate the contribution of other sources of O_2^- production other than NAPDH oxidase, cells were preincubated for 30 min with rotenone (100 μM, inhibitor of mitochondrial complex I activity), indomethacin (10 μM, inhibitor of cyclooxygenase), oxypurinol (100 μM, inhibitor of xanthine oxidase), and N^G-nitro-L-arginine methyl ester (L-NAME; 100 μM, inhibitor of nitric oxide synthases) before O_2^- measurements by using lucigenin chemiluminescence.

Subcellular fractionation

Confluent human myoblasts were washed twice with ice-cold PBS and lysed on ice in HEPES buffer (HEPES, 50 m*M*; NaCl, 150 m*M*; NaF, 100 m*M*; EDTA, 5 m*M*; and triton X-100, 0.5%) containing protease inhibitors (aprotinin, 5mg/ml; leupeptin, 2 mg/ml; and PMSF, 100 m*M*) and sonicated at 100W for 15 sec on ice. The homogenate was centrifuged at 250 *g* for 5 min followed by 20-min centrifugation at 20,000 *g* to separate the mitochondria. The supernatant was then centrifuged for 60 min at 100,000 *g* to obtain detergent-resistant proteins in the pellet and detergent-soluble proteins in the supernatant. All fractions were stored at -80°C until further analysis.

Transfection with plasmids and fluorescence microscopy

To identify subcellular targeting of NADPH oxidase subunit proteins in human skeletal myoblasts, expression vectors containing enhanced cyan (ECFP), and enhanced yellow (EYFP) fluorescence proteins were used following methods for the construction of ECFP-Nox2, EYFP-p22^{phox}, and EYFP-Nox4 expression vectors that were previously described (32). ECFP-p47^{phox} and EYFP-p67^{phox} expression vectors were generated by cloning human p47^{phox} and p67^{phox} cDNA into pECFP-C1 and pEYFP-C1 vectors, respectively (BD Biosciences Inc., Mississauga, ON, Canada). Expression vectors for subcellular localization markers; pECFP-ER for endoplasmic reticulum, pECFP-Mito for mitochondria, pECFP-Peroxi for peroxisomes, and pECFP-Endo for endosomes were obtained from Clontech (Palo Alto, CA). These vectors encode fusion proteins consisting of ECFP and targeting sequences of calreticulin (ER), subunit VIII of cytochrome *c* oxidase (mitochondria), peroximal targeting signal 1 (peroxisomes), and rhoB GTPase (endosomes), respectively. Transient transfections were performed

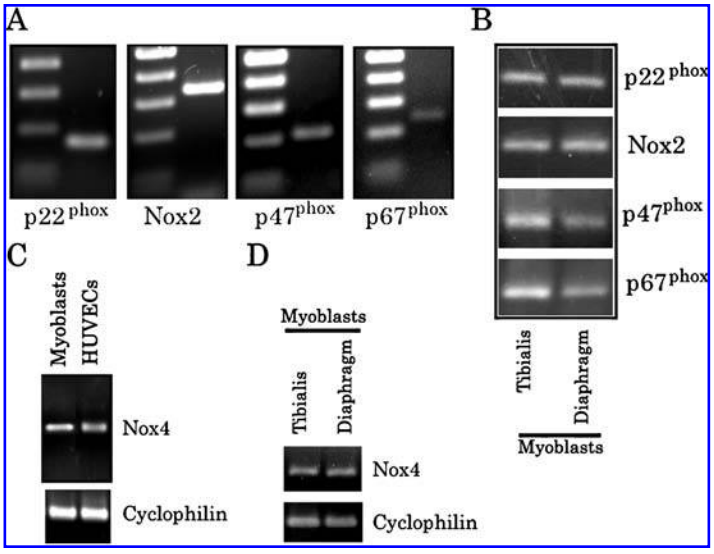

FIG. 1. (A) RT-PCR amplification of p22^{phox}, Nox2, p47^{phox}, and p67^{phox} transcripts in human skeletal myoblasts. In each panel, PCR products are shown on the right side, whereas the DNA ladder is shown to the left. (**B**) RT-PCR amplification of p22^{phox}, Nox2, p47^{phox}, and p67^{phox} transcripts in mouse tibialis anterior and diaphragm muscles. (**C**, **D**) Amplification of Nox4 mRNA by using RT-PCR in human myoblasts (**C**) and in murine myoblasts derived from diaphragm and tibialis anterior muscles (**D**). Human umbilical vein endothelial cells (HUVECs) were used as positive controls.

TABLE 3. EXPRESSION OF MRNA OF VARIOUS NADPH OXIDASE SUBUNITS IN SKELETAL MYOBLASTS EXPRESSED IN COPIES/NG TOTAL RNA

	Gp91^{phox}/Nox2	*p22^{phox}*	*p47^{phox}*	*p67^{phox}*	*Nox4*
Primary human myoblasts	0.1*	1444	0.05*	0.3*	16*
Primary mouse diaphragm myoblasts	0.8*	1260	0.1*	0.3*	42*
Primary mouse tibialis myoblasts	0.2*	426	0.1*	0.3*	13*
C2C12 myoblasts	0.7*	0.1	0.03*	6.1*	42*

Values are means of four independent samples.
*$p < 0.05$ compared with p22^{phox} (using Two-Way ANOVA).

with human skeletal myoblasts cells seeded on 22-mm^2 cover slips in 24-well tissue-culture plates by using Lipofectamine LTX (Invitrogen) at a 1:2 ratio of DNA/Lipofectamine in Opti-MEM I Medium (Invitrogen), in accordance with the manufacturer's recommendations. Fluorescence was visualized 48 h later by using a Zeiss LSM-510 META laser scanning microscope with a 40× oil immersion lens in a multitrack mode with dual excitation (458 nm for ECFP and 514 nm for EYFP) and emission (BP 470–500 nm for ECFP, and BP 530–600 nm for EYFP) filter sets.

Adenoviral infection of myoblasts

Human skeletal myoblasts (15×10^4) were seeded in 24-well plates and infected for 5 h with adenoviruses (multiplicity of infection was 500–1,500) in basal medium. These conditions resulted in uniform expression of transgenes in ~90% of the cells, as assessed by green fluorescence protein (GFP) fluorescence. The viruses were then removed, and cells were allowed to recover in complete medium for 24 h. To inhibit p47^{phox}, adenoviruses expressing a mutant form of p47^{phox}, which is defective in the first Src homology 3 (SH3) domain [p47W(193)R], were used (15). To evaluate the functional importance of Nox4, myoblasts were infected with dominant-negative Nox4 adenoviruses lacking FAD-NAD(P)H binding domains (Ad-ΔFAD/NADPH-Nox4), which were generously provided by B.J. Goldstein (Thomas Jefferson University, Philadelphia, PA) (29). To evaluate involvement of the NF-κB pathway in myoblast proliferation, myoblasts were infected with adenoviruses expressing dominant-negative mutant forms of IκB kinase (IKK) α (Ad-dnIKKα) and IKKβ (Ad-dnIKKβ), as previously described (34). Adenoviruses expressing GFP were used as controls in all experiments involving adenoviruses.

Transfection with small inhibitory RNA (siRNA) oligonucleotides

Double-stranded siRNA oligos targeting the 5′-AAT TAC TAT GTT CGG GCC GTC-3′ region of the human p22^{phox} coding sequence were synthesized and purified by Qiagen. To inhibit Nox4 expression, we used a pool of three commercially designed siRNA oligos (Dharmacon Inc., Chicago, IL). A fluorescein-labeled nonsilencing control siRNA oligo (Alexa Fluor488; Qiagen) was used as a control. Myoblasts were transfected with siRNA oligos by using HiPerFect Transfection Reagent (Qiagen) in skeletal muscle growth serum (SkGM) and were examined 24 h later for mRNA expression and 48 h later for protein expression.

Myoblast proliferation

Myoblast proliferation was assessed by using two different assays: cell count and bromodeoxyuridine (BrdU) incorporation. For the cell count, myoblasts (15×10^5 cells) were plated into 12-well plates and maintained for 24 h in complete culture medium containing 15% FBS in the absence and presence of NAC (10 m*M*), apocynin (1 m*M*), PI-3 kinase inhibitors (LY294002 at 300

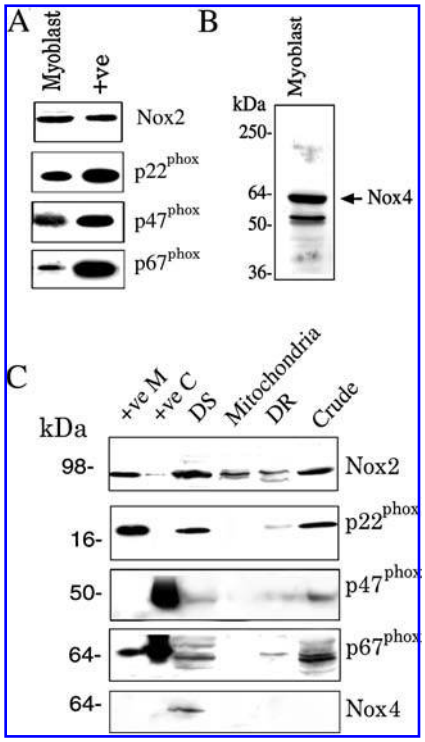

FIG. 2. (A, B) Detection of Nox2, p22^{phox}, p47^{phox}, p67^{phox}, and Nox4 in total cell lysates of human myoblasts using immunoblotting and selective antibodies. +, Human neutrophil lysates. (**C**) Expression of NADPH oxidase subunits in crude lysates, detergent-soluble (DS), mitochondrial, and detergent-resistant (DR) fractions of human myoblasts. +M and +C, Membrane and cytosolic fractions of human neutrophils.

n*M* and wortmannin at 100 n*M*), a mammalian target of the rapamycin (mTOR) pathway inhibitor (rapamycin at 50 ng/ml), an Erk1/2 inhibitor (PD98059 at 30 μM), and an NF-κB inhibitor (BAY11-7082 at 1 μM). Cells were then trypsinized (0.5% trypsin-EDTA) and stained with trypan blue. Viable cells were counted by hematocytometer. For BrdU incorporation, a Cell Proliferation ELISA, BrdU colorimetric kit was used (Roche Applied Science, Laval, Quebec, Canada). Myoblasts were plated into 96-well plates at a density of 5×10^3 cells/well in 100 μl of full culture medium for 24 h in the absence and presence of antioxidants and various inhibitors. Cells were then pulsed with 10 μM BrdU for 4 h, fixed and then labeled, according to the manufacturer's instructions. Absorbance (370 nm) was measured 10 min after the addition of substrate.

Immunoblotting

Crude cell lysates or cell fractions (30 to 80 μg total protein) were boiled for 5 min and then loaded onto tris-glycine SDS-polyacrylamide gels. Proteins were electrophoretically transferred onto polyvinylidene difluoride membranes, blocked for 1 h with 5% nonfat dry milk, and incubated overnight at 4°C with primary antibodies. Nox2, $p47^{phox}$, and $p67^{phox}$ proteins were detected with polyclonal antibodies (22), whereas $p22^{phox}$ protein was identified by using a monoclonal antibody (mAb48), generously provided by Dr. D. Roos (University of Amsterdam, The Netherlands). Nox4 protein was detected with an affinity-purified polyclonal antibody (13). Activation of Erk1/2 was assessed with polyclonal antibodies specific to active (dually phosphorylated at $Thre^{183}$ and Tyr^{185}) and total Erk1/2. The p38 and stress-activated protein kinase/c-Jun NH_2-terminal kinase (SAPK/JNK) phosphorylation was monitored with polyclonal phospho-p38 ($Thre^{180}/Tyr^{182}$), phospho-SAPK/JNK ($Thre^{183}/Tyr^{185}$), and total p38 and total SAPK/JNK antibodies. Phosphorylation of the p65 subunit of NF-κB (RelA) was assessed by using a phospho-Ser^{536} antibody. Phosphorylation of mTOR at Ser^{2448} and AKT at Ser^{473} was detected with polyclonal antibodies. All antibodies were purchased from Cell Signaling Technology (Danvers, MA). Myogenin (A4.74) and myosin heavy-chain (MF20) protein levels were assessed by using monoclonal antibodies (Developmental Studies Hybridoma Bank, University of Iowa). Proteins were detected with horseradish peroxidase–conjugated anti-mouse or anti-rabbit secondary antibodies and ECL reagents (Chemicon Inc., Temecula, CA). Blots were scanned with an imaging densitometer, and optical densities of the protein bands were quantified with ImagePro software (Media Cybernetics, Carlsbad, CA). Predetermined molecular weight standards were used as

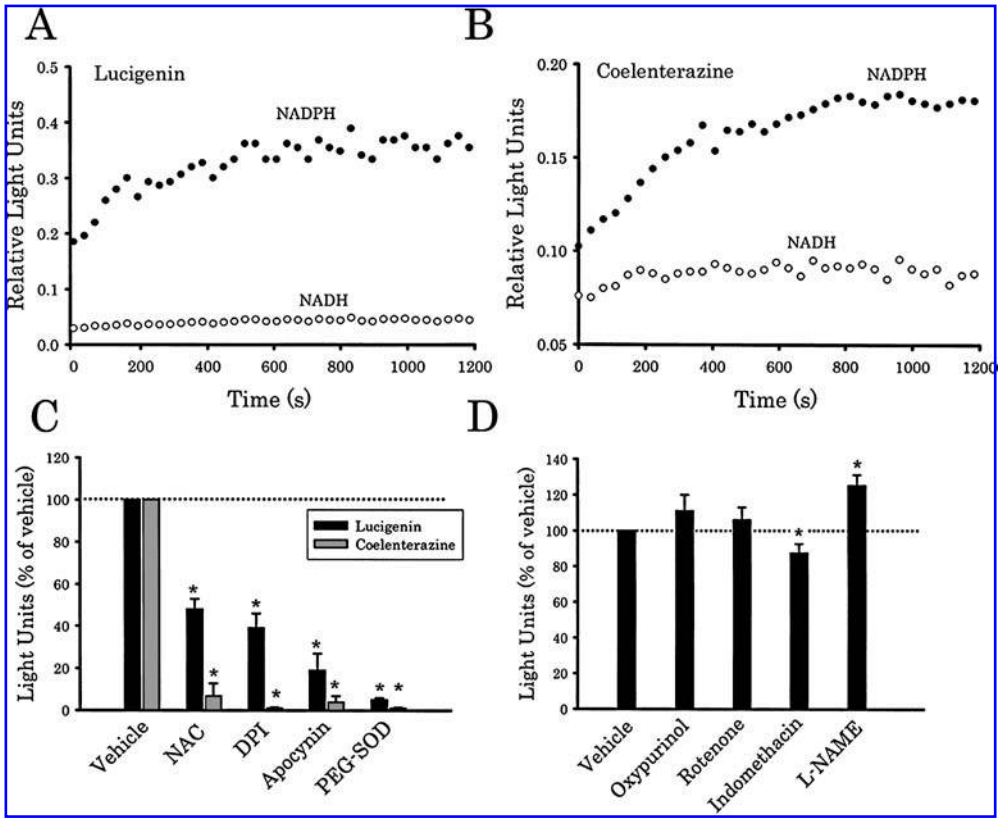

FIG. 3. (A, B) Representative examples of O_2^- production in the presence of NADPH and NADH in human myoblasts measured with lucigenin (A) and coelenterazine (B) chemiluminescence. (**C**) Effects of NAC, DPI, apocynin, and PEG-SOD on O_2^- production in human myoblasts. Values were obtained with lucigenin and coelenterazine chemiluminescence and are expressed as percentage of those measured in the presence of vehicle (DMSO). (**D**) Effects of oxypurinol, rotenone, indomethacin, and L-NAME on O_2^- production (measured with lucigenin chemiluminescence) in human myoblasts. $^*p < 0.05$ compared with vehicle.

markers. Protein concentration was measured by the Bradford method, with bovine serum albumin as a standard.

Measurement of serum-induced proliferation in myoblasts

To evaluate the mechanisms through which oxidants influence serum-induced proliferation of human skeletal myoblasts, the activation status of the p38 and Erk1/2 members of mitogen-activated protein kinases (MAPKs), protein kinase B (AKT), mTOR, and NF-κB pathways were measured. Subconfluent human skeletal myoblasts plated into six-well plates were serum starved for 4 h in serum-free medium (SkBM) and then exposed to 15% FBS for 5, 15, and 60 min. Cells were then lysed and underwent immunoblotting for total and phosphorylated p38, Erk1/2, AKT, mTOR, and the p65 subunit of NF-κB. Some serum-starved myoblasts were stimulated for 15 min with 15% FBS in the presence 0.02% dimethyl sulfoxide (DMSO, vehicle), NAC (10 m*M*), or apocynin (1 m*M*). Cells were then collected, and phosphorylation of the previously mentioned pathways was evaluated by using immunoblotting.

Data analysis

Results are shown as means ± SEM. For immunoblotting experiments, at least three independent measurements were performed within each group. Six independent measurements of cell proliferation and O_2^- production were performed. Comparisons of ROS generation between vehicle-treated cells and those treated with various inhibitors and ROS generation between myotubes and myoblasts were performed with a one-way analysis of variance where probability (p) values <0.05 were considered significant. Similar analysis was used to compare the effects of vehicle *versus* apocynin and NAC on cell number and BrdU incorporation and the effects of scrambled siRNA oligos *versus* Nox4 and p22^{phox} siRNA oligos and GFP *versus* dominant negative forms of p47^{phox} and Nox4 on these parameters. For comparison of NAPDH oxidase mRNA abundance between various mouse muscles and between different types of primary muscle precursor cells, we used two-way analysis of variance where probability (p) values <0.05 were considered significant.

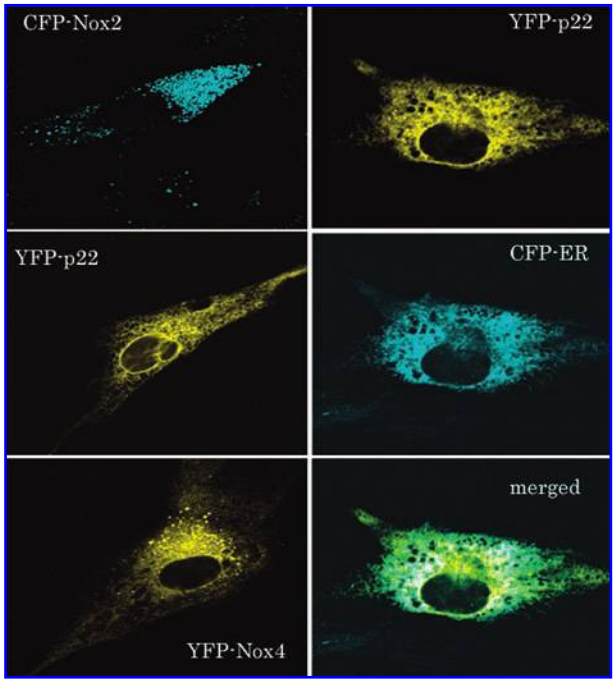

FIG. 4. Intracellular localization of fusion proteins of Nox2, Nox4, and p22^{phox} in human myoblasts. In few experiments, cells were double-transfected with p-EYFP-p22^{phox} and p-ECFP-ER vectors (see Methods). Note the endoplasmic reticulum–like distribution of Nox2, Nox4, and p22^{phox}. This was confirmed by cotransfection of p-EYFP-p22^{phox} and p-ECFP-ER vectors in the same cells. (For interpretation of the references to color in this figure legend, the reader is referred to the web version of this article at www.liebertonline.com/ars).

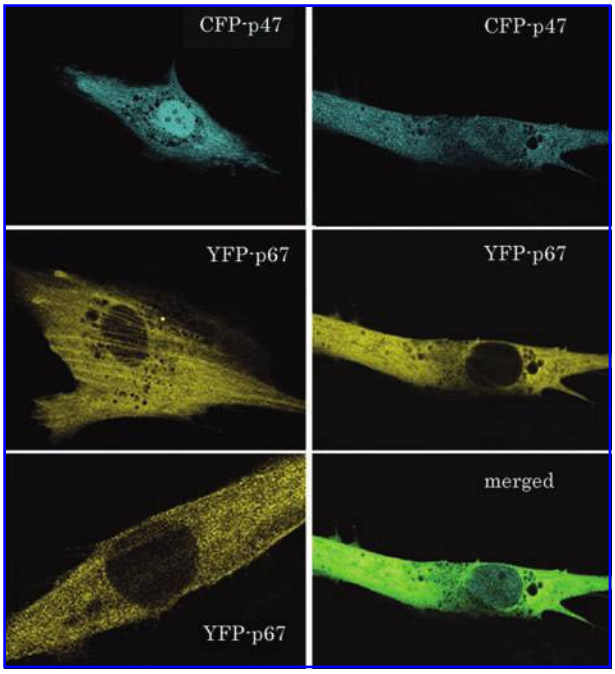

FIG. 5. Intracellular localization of fusion proteins of p47^{phox} and p67^{phox}. Note the diffuse cytosolic distribution of p47^{phox} and p67^{phox}. Also note the nuclear localization of p47^{phox} *(upper right)* and membrane-associated distribution of p67^{phox} *(lower right*). (For interpretation of the references to color in this figure legend, the reader is referred to the web version of this article at www.liebertonline.com/ars).

RESULTS

Expression of NADPH oxidase subunits

Transcripts of Nox2, Nox4, p22^{phox}, p47^{phox}, and p67^{phox} subunits were detected in the diaphragm, EDL, and tibialis anterior and soleus muscles of normal mice by using RT-PCR. Table 2 lists the expression levels of these subunits expressed as copies per nanogram total RNA and reveals two main observations: First, the abundance of NADPH oxidase subunits in the diaphragm was relatively higher than that measured in other muscles; second, in a given muscle, the p22^{phox} subunit was the most abundant, as compared with other subunits. Transcripts of

Nox2, Nox4, p22^{phox}, p47^{phox}, and p67^{phox} subunits were also detected in primary human and murine muscle precursor cells (myoblasts) derived from the diaphragm and tibialis anterior muscles (Fig. 1). In these cells, the relative abundance of the p22^{phox} mRNA was substantially higher than in other subunits. Nox4 was the second most abundant subunit in terms of mRNA expression (Table 3). In addition, between murine and human myoblasts, relative mRNA expressions of NADPH oxidase subunits were similar, although murine C2C12 myoblasts showed substantially lower p22^{phox} mRNA expression than did primary myoblasts (see Table 3). No detectable mRNA transcripts of Nox1, Nox3, and Nox5 were observed in either murine or human myoblasts (data not shown). Immunoblotting analysis of primary murine and human myoblasts using specific antibodies confirmed the presence of 91-, 22-, 47-, and 67-kDa protein bands equivalent to Nox2, p22^{phox}, p47^{phox}, and p67^{phox} subunits, respectively (Fig. 2A). In addition, anti-Nox4 antibody detected a strong band at 64 kDa, which disappeared when the antibody was preincubated with the immunizing peptide. A nonspecific band was also detected at 55 kDa (Fig. 2B).

Localization of NADPH oxidase

Fractionation of human myoblast lysates into subcellular fractions revealed the presence of Nox2, Nox4, p22^{phox}, p67^{phox}, and p47^{phox} proteins in the detergent-soluble fraction. Only weak expressions of Nox2, p67^{phox}, and p47^{phox} were detected in the detergent-resistant fraction (Fig. 2C). Nox2 protein was also detected in the mitochondrial fraction (Fig. 2C).

Production of O_2^-

Measurements of O_2^- anion levels in human myoblasts using lucigenin and coelenterazine chemiluminescence revealed an activity that was dependent on the presence of NADPH rather than NADH (Fig. 3A and B). Preincubation with PEG-SOD, NAC, DPI, or apocynin for 1 h significantly attenuated O_2^- production in these cells (Fig. 3C). In addition, inhibition of mitochondrial complex I and xanthine oxidases with rotenone and oxypurinol, respectively, had no effects on O_2^- production. By comparison, indomethacin (inhibitor of cyclooxygenases) mildly attenuated O_2^- production, whereas L-NAME (inhibitor of nitric oxide synthases) significantly enhanced O_2^- levels (Fig. 3D).

Localization of NAPDH oxidase fusion proteins

To investigate the targeting of NADPH oxidase subunits to various intracellular compartments, human myoblasts were transfected with vectors that express ECFP and EYFP fused to

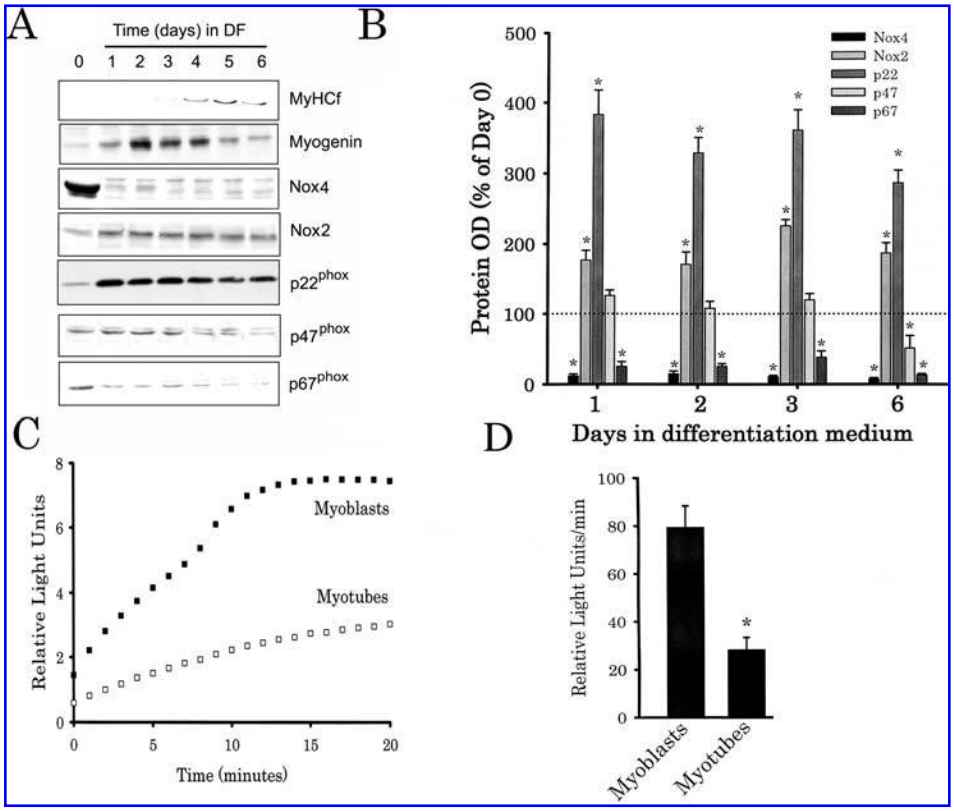

FIG. 6. (A, B) Regulation of NADPH oxidase expression during myoblast differentiation into myotubes. Myoblasts grown in differentiation medium (DF) for 1–6 days, and expression of NADPH oxidase subunits, myogenin, and myosin heavy-chain (MyHCf) proteins measured with immunoblotting. Day 0 designates undifferentiated myoblasts. Representative immunoblots are shown in (**A**). Mean values of protein optical density (expressed as percentage of those measured in myoblasts) are shown in (**B**). (**C, D**) Representative and mean values of O_2^- production ($n = 4$) in proliferating myoblasts and differentiated myotubes (day 6) by using lucigenin-enhanced chemiluminescence.

NADPH oxidase subunit proteins. Nox2, Nox4, and $p22^{phox}$ proteins primarily exhibited an endoplasmic (ER)-like expression pattern (Fig. 4). In addition, nuclear membranes stained positive for $p22^{phox}$ (see Fig. 4). This was confirmed by using the ECFP-ER vector, which encodes a fusion protein with ECFP and calreticulin (localized in the ER; see Fig. 4). The $p67^{phox}$ protein was localized to the cytosol in a pattern similar to that of the cytoskeleton, with weak membrane-associated staining evident in a few cells (Fig. 5). In comparison, diffuse cytosolic staining in addition to strong nuclear staining was detected for the $p47^{phox}$ fusion protein (see Fig. 5).

NADPH oxidase expression and myoblast differentiation

Differentiation into myotubes was induced by incubation of myoblasts in differentiation medium (DMEM plus 2% HS) and was associated with the appearance of myogenin transcription factor and myosin heavy-chain protein within 1 and 4 days, respectively (Fig. 6A). Differentiation into myotubes elicited a rapid decline in Nox4 and $p67^{phox}$ levels, a slower reduction in $p47^{phox}$ expression, and a rapid increase in $p22^{phox}$ and Nox2 expression (see Fig. 6A and B). In addition, differentiation into myotubes was associated with a significant decline in O_2^- production, as measured by lucigenin-enhanced chemiluminescence (Fig. 6C and D).

Regulation of cell proliferation by ROS

Figure 7 shows that NAC and apocynin significantly attenuated cell number and BrdU incorporation in skeletal myoblasts grown for 24 h in the presence of 15% FBS ($p < 0.05$ compared with vehicle). Transfection with $p22^{phox}$ siRNA oligonucleotides reduced $p22^{phox}$ protein expression by 75%, attenuated myoblast O_2^- production, and reduced cell number and BrdU incorporation by 26 and 24%, respectively (Fig. 8). Similarly, expression of dominant-negative $p47^{phox}$ [p47W(192)R] protein attenuated O_2^- production, cell number, and BrdU incorporation, as compared with cells expressing GFP (Fig. 9). Finally, expression of dominant-negative Nox4 (ΔFAD/NADPH Nox4) protein also attenuated O_2^- production and significantly reduced BrdU incorporation by 26% in human myoblasts (Fig. 10). Similarly, transfection of myoblasts with Nox4 siRNA oligos attenuated Nox4 protein expression and reduced cell number by about 29% (see Fig. 10).

To evaluate the pathways involved in serum-induced proliferation of myoblasts and the influence of NADH oxidase–derived ROS on these pathways, serum-starved myoblasts were first exposed to 15% FBS, which triggered a rapid (within 5min) increase in phosphorylation of p38, Erk1/2, AKT, and mTOR proteins and a delayed (within 60 min) augmentation of phosphorylation of the p65 subunit of NF-κB (Fig. 11A). Serum-induced phosphorylation of Erk1/2, AKT, mTOR, and p65 NF-κB proteins was significantly attenuated, whereas that of p38 protein increased substantially when NAC and apocynin were present (Fig. 11B and C). These results indicate that serum-induced activation of the Erk1/2, PI-3 kinase/AKT, mTOR, and the p65 NF-κB pathways is redox sensitive. To evaluate the roles of these pathways in myoblast proliferation, cell counting of myoblasts cultured in full culture medium in the presence of

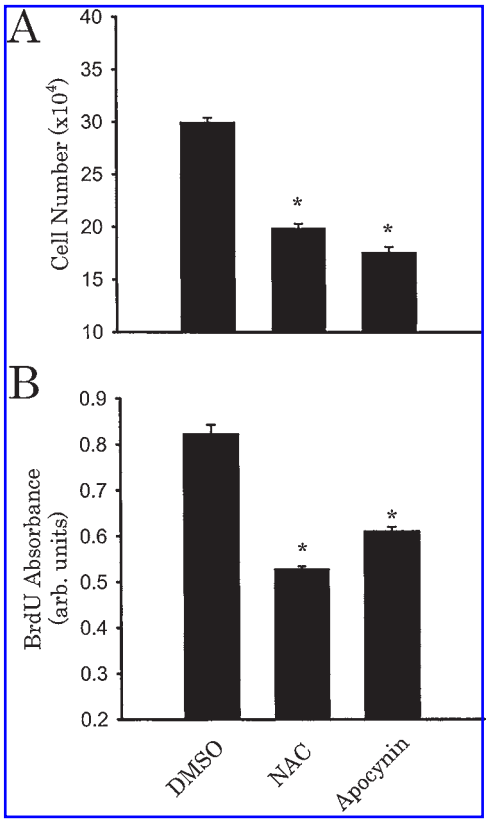

FIG. 7. Regulation of proliferation in human skeletal myoblasts grown for 24 h in full medium in the presence of DMSO (vehicle), NAC, or apocynin. Cell count and BrdU incorporation mean values are shown in (**A**) and (**B**). *$p < 0.05$ compared with DMSO.

DMSO (vehicle) or selective inhibitors of Erk1/2 (PD98059), PI-3 kinase (wortmannin and LY924002), mTOR (rapamycin), and NF-κB (Bay11-7082) pathways was performed. All inhibitors significantly attenuated cell numbers, as compared with cells treated with vehicle (Fig. 11D). In addition, expression of dominant-negative IKKα and IKKβ proteins significantly reduced cell counts, as compared with cells expressing GFP (Fig. 11D). Previous studies confirmed that oxidants regulate cell proliferation in response to serum or mitogen exposure by inducing the expression of cyclin D1, a protein that induces the transition of the cell cycle from the quiescent G_0 phase to G_1 phase. Figure 12 indicates that this was the case in human skeletal myoblasts, where $p22^{phox}$ expression was knocked down by using siRNA oligonucleotides or where inhibition of $p47^{phox}$ and Nox4 activities using dominant-negative forms resulted in significant attenuation of cyclin D1 expression.

DISCUSSION

The main findings of this study are as follows: (a) The NADPH oxidase subunits Nox2, Nox4, $p22^{phox}$, $p47^{phox}$, and $p67^{phox}$ are expressed in murine skeletal muscles and in primary murine and human skeletal muscle precursor cells (myoblasts); (b) NADPH oxidase–fusion proteins are localized in the

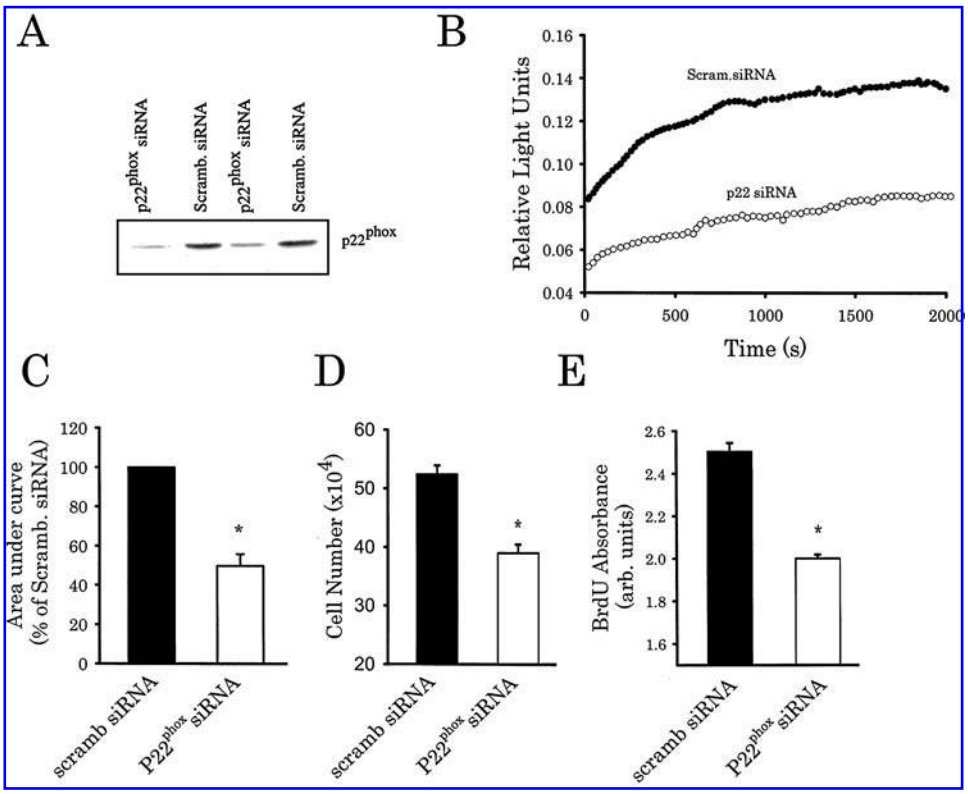

FIG. 8. Expression of p22^{phox} (A), O_2^- production (B, C), cell count (D), and BrdU incorporation (E) in human myoblasts transfected with siRNA oligonucleotides selective to p22^{phox} or scrambled siRNA oligonucleotides. *$p < 0.05$ compared with cells transfected with scrambled siRNA oligonucleotides.

endoplasmic reticulum, membrane, and nuclear compartments; (c) both Nox2 and Nox4 contribute to O_2^- production in proliferating human skeletal myoblasts, whereas the contribution of Nox4 is reduced significantly during differentiation of myoblasts to myotubes; and (d) NADPH oxidase–derived oxidants promote myoblast proliferation through activation of the Erk1/2, PI-3 kinase/AKT, mTOR, and NF-κB pathways, eventually resulting in the induction of cyclin D1 expression and progression of the cell cycle.

Methodologic considerations

The use of lucigenin chemiluminescence as a measure of O_2^- production in cellular preparations has been criticized because of the generation of O_2^- radicals by redox recycling of lucigenin itself, particularly when used at relatively high concentrations (27). We propose that redox recycling did not contribute to lucigenin chemiluminescence signals measured in our study for the following reasons: (a) we used lucigenin at 10 μM, a concentration that is not associated with redox recycling (26); (b) measurements of O_2^- production in myoblasts by using coelenterazine, which does not undergo redox recycling, produced similar patterns than those measured with lucigenin (see Fig. 3); (c) pharmacologic (DPI and apocynin) and molecular (siRNA oligos and dominant-negative proteins) inhibition of NAPDH oxidase significantly attenuated lucigenin chemiluminescence signals. We should emphasize that although we used an assay in which NADPH or NADH was added to intact cells, it remains unclear exactly how this affects NADPH oxidase activity. Nevertheless, previous studies suggest that this assay correlates quite well with NADPH oxidase assays performed in cell homogenates.

Expression of NADPH oxidase in skeletal muscles

Little information is available regarding the activity and functional significance of NADPH oxidase in skeletal muscles. Our group was the first to report the presence of Nox2, p47^{phox}, p67^{phox}, and p22^{phox} proteins in rat skeletal muscle samples (22). More recently, Hidalgo *et al.* (20) identified Nox2, p47^{phox}, p67^{phox}, and p22^{phox} proteins in the transverse tubules of mouse and rabbit skeletal muscles and proposed that oxidants derived from NADPH oxidase activate ryanodine receptors through redox modifications. Our results (see Table 2) confirm that murine skeletal muscles contain not only Nox2, but also Nox4 protein in addition to p22^{phox}, p47^{phox}, and p67^{phox}. Furthermore, we report here that the relative mRNA expression of all NADPH oxidase subunits in the diaphragm is higher than that in limb muscles (see Table 2). Although the reasons behind this particular distribution of NADPH oxidase mRNA expression remain unclear, we speculate that many factors such as myosin heavy-chain composition, vascularity, and the pattern of muscle recruitment might be important factors in determining NAPDH oxidase abundance. For example, myosin heavy-chain composition, which influences many aspects of skeletal muscle physiology, is different among the muscles

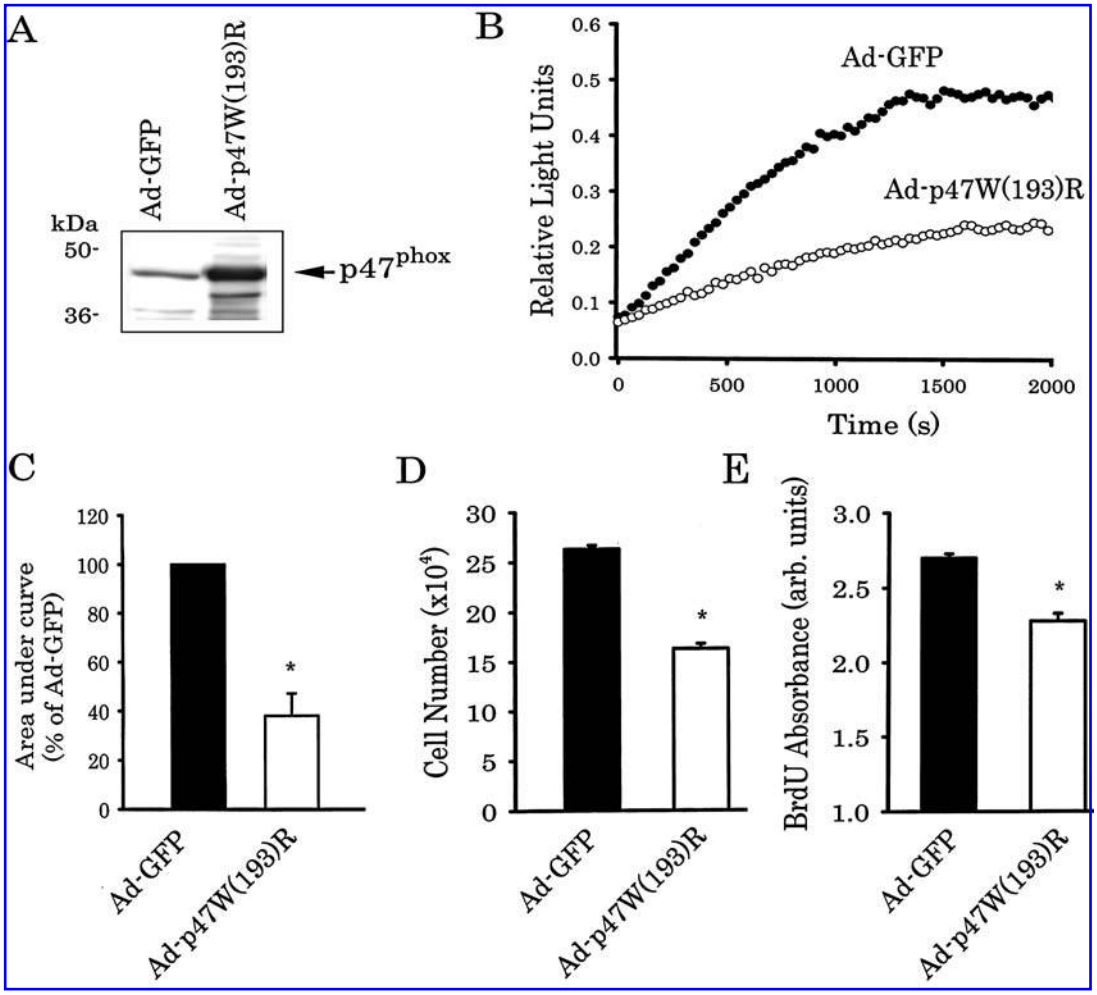

FIG. 9. Expression of p47^{phox} (A), O_2^- production (B, C), cell count (D), and BrdU incorporation (E) in human myoblasts infected with adenoviruses expressing GFP or a dominant-negative form of p47^{phox} (p47W193R). *$p < 0.05$ compared with cells infected with GFP adenoviruses.

listed in Table 2. The diaphragm and soleus muscles express mainly type I myosin heavy-chain isoform (39). Both of these muscles have relatively higher abundance of NAPDH oxidase subunits compared with the EDL and tibialis anterior muscles, which express mainly type 2 myosin heavy-chain isoform (see Table 2). In addition, vascular cells also could have contributed to total NAPDH oxidase expression of intact muscle samples. These cells express Nox1, Nox2, and Nox4 in addition to p22^{phox}, p67^{phox}, and p47^{phox} (23). Relatively higher NAPDH oxidase expression in the diaphragm and soleus muscles could, therefore, be attributed in part to higher capillary densities in these muscles compared with the EDL and tibialis anterior muscles (11). Finally, it is also possible that elevated NADPH oxidase expression in the diaphragm might be an adaptive response designed to provide an abundance of ROS to facilitate optimal Ca^{2+} release from ryanodine receptors during repetitive activation of the diaphragm across breathing cycles.

Another important finding regarding NADPH oxidase expression in murine skeletal muscles is that the relative abundance of the p22^{phox} mRNA in various murine skeletal muscles is substantially higher than that of other subunits (see Table 2). We attribute this finding to the fact that p22^{phox} protein binds to more than one Nox isoform, and its presence is required for stabilization and optimal activity of Nox proteins, except for Nox5 (23). The presence of two Nox proteins (Nox2 and Nox4) inside muscle fibers would, therefore, justify the relatively high abundance of p22^{phox} subunits in these fibers. However, assuming 1:1 stoichiometry in the NADPH oxidase complex, the relatively high abundance of p22^{phox} mRNA could not simply be explained by the association of this subunit with more than one Nox isoform. An alternative explanation for the relatively high abundance of p22^{phox} mRNA expression in muscle precursor cells is that this protein may have functions other than regulation of Nox-derived ROS production. The nature of these functions remains to be elucidated.

As in skeletal muscle fibers, little is known regarding the structure and biologic roles of NADPH oxidase in skeletal muscle satellite cells. Two recent studies confirmed the presence of Nox2, p47^{phox}, and p67^{phox} mRNA and proteins in immortalized rat L6 myoblasts and myotubes and also reported the involvement of NADPH oxidase-derived ROS in insulin signaling and Ca^{2+} flux (12, 41). Others, however, have failed to

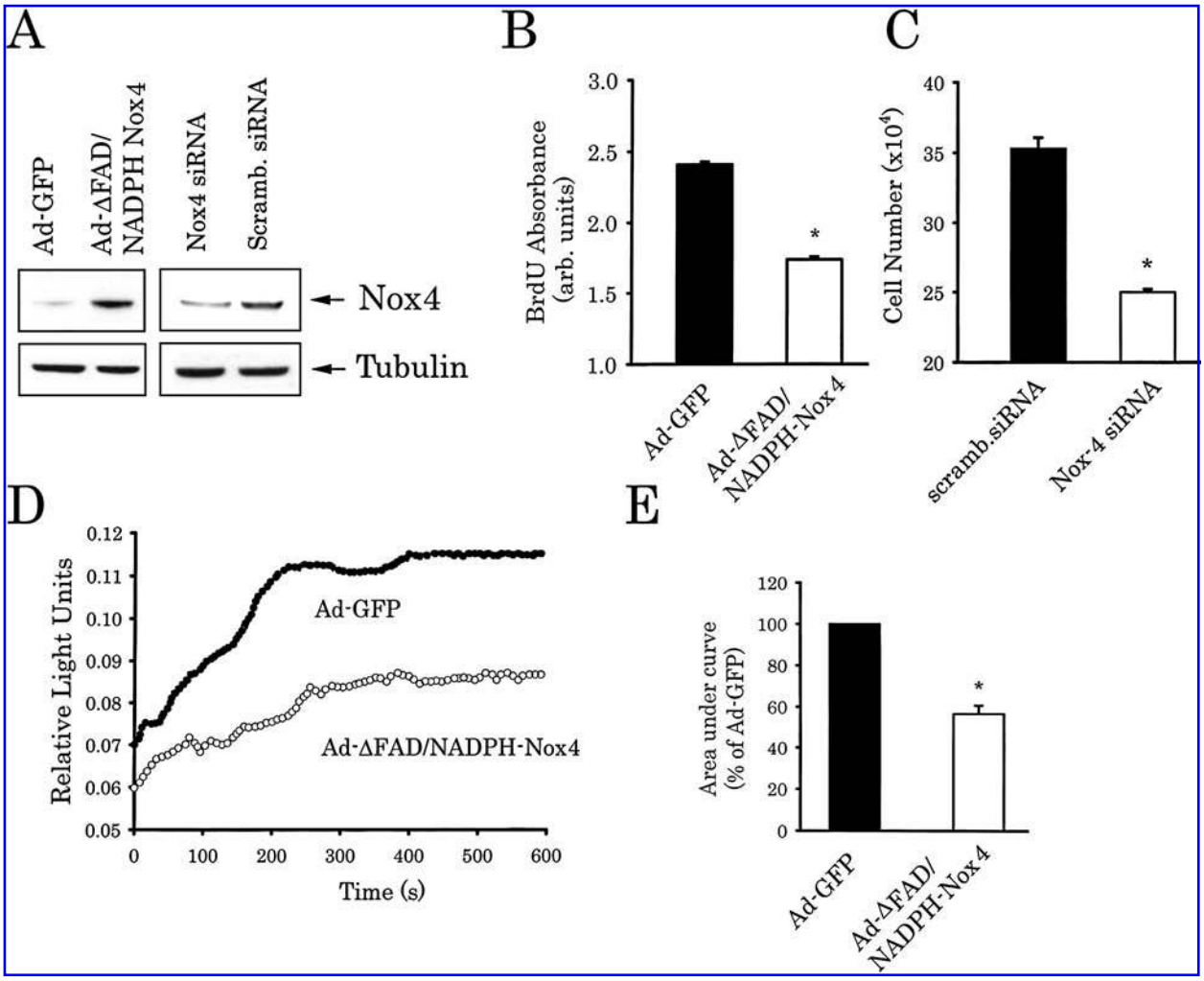

FIG. 10. (A) Expression of Nox4 protein in human myoblasts infected with adenoviruses expressing GFP and dominant-negative Nox4 (ΔFAD/NADPH Nox4) and in myoblasts transfected with scrambled and Nox4 siRNA oligos. (**B**) BrdU incorporation in myoblasts infected with GFP and dominant negative Nox4 viruses. (**C**) Cell number after 48 h of transfection with scrambled and Nox4 siRNA oligos. (**D, E**) Representative and mean values of O_2^- production (measured with lucigenin chemiluminescence) in human myoblasts infected with GFP and dominant-negative Nox4 viruses. $^*p < 0.05$ compared with cells infected with GFP adenoviruses and cells transfected with scrambled siRNA oligos.

detect mRNA expression of Nox4, Nox2, $p22^{phox}$, and $p47^{phox}$ in C2C12 and L6 immortalized murine myoblasts but have detected $p47^{phox}$ and Nox4 mRNA in primary skeletal myoblasts (21). The present study indicates that primary human and murine myoblasts derived from the diaphragm and tibialis anterior muscles express both Nox2 and Nox4, in addition to $p22^{phox}$, $p47^{phox}$, and $p67^{phox}$ at mRNA and protein levels. These results suggest that failures to detect NADPH oxidase expression in immortalized myoblasts from C2C12 and L6 origins might be due to the relatively low expression of oxidase subunits, particularly $p22^{phox}$. These cells may not, therefore, be ideally suited to the study of the biologic roles of the NADPH oxidase (see Table 3).

Although we did not use immunocytochemistry to assess subcellular localization of endogenous Nox isoforms and subunits, we attempted to identify intracellular localization of the NADPH oxidase by using two indirect approaches: subcellular fractionation and expression of NADPH oxidase fluorescent-fusion proteins. Both approaches revealed prominent ER-like distributions for Nox2, Nox4, and $p22^{phox}$ and more diffuse staining for $p47^{phox}$ and $p67^{phox}$ (see Figs. 4 and 5). We also identified membrane-associated Nox2, $p47^{phox}$, and $p67^{phox}$ (Fig. 5). The ER-like distribution of Nox2, Nox4, and $p22^{phox}$ in proliferating myoblasts is similar to that reported in endothelial cells (32). Moreover, the membrane-related expression of NADPH oxidase subunits in the present study is similar to that described at the leading edge of migrating endothelial cells, suggesting that, as in vascular cells, NADPH oxidase–derived ROS may be involved in regulating myoblast motility (42). Another interesting observation in the present study is that $p47^{phox}$ fluorescence fusion protein was frequently detected in the nuclei of human skeletal myoblasts (see Fig. 5). Although the mechanisms and functional significance of this nuclear localization remain to be determined, we speculate that $p47^{phox}$ is

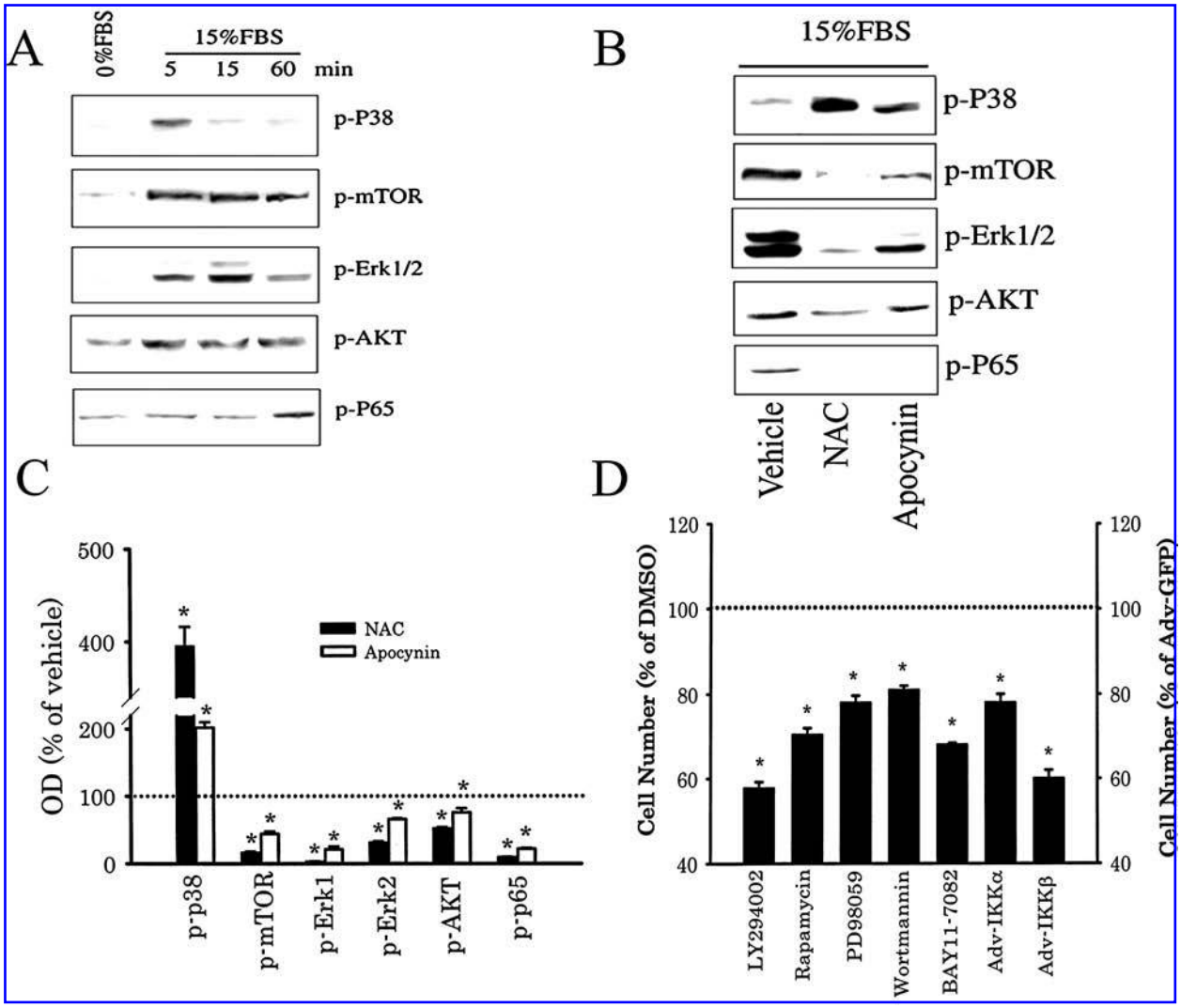

FIG. 11. (A) Phosphorylation of p38, mTOR, Erk1/2, AKT, and the p65 subunit of NF-κB after 5, 15, and 60 min of addition of 15% FBS in serum-starved human myoblasts. (**B, C**) Influence of vehicle (DMSO), NAC, and apocynin on the intensity (representative example in **B** and mean values in **C**) of p38, mTOR, Erk1/2, AKT, and p65 NF-κB phosphorylation measured after 15 min of serum exposure in serum-starved myoblasts. (**D**) Influence of inhibitors of PI-3 kinase (LY294002, wortmannin), mTOR (rapamycin and LY294002), Erk1/2 (PD98059), and NF-κB (Bay11-7082 and dominant-negative forms of IKKα and IKKβ) pathways on myoblast cell number counted after a 24-h period. Results are normalized as percentage of values measured in the presence of vehicle (DMSO) or in cells infected with GFP viruses.

targeted to the nucleus because of specific interactions of the tandem SH3 domains of $p47^{phox}$ with the proline-rich mid region of the p65 subunit of NF-κB (RelA) (14). This association results in potentiation of NF-κB activation in response to IL-1β exposure (14).

Contribution of NADPH oxidase subunits to O_2^- production

The present study reveals for the first time that both Nox2 and Nox4 contribute to O_2^- production in proliferating human skeletal myoblasts. This conclusion is based on the observations that knocking down $p22^{phox}$ expression by using siRNA and inhibiting $p47^{phox}$ and Nox4 activities by using dominant-negative proteins attenuates O_2^- production in proliferating human myoblasts (see Figs. 8–10). However, the differential contribution of Nox2 and Nox4 to total O_2^- production in myoblasts remains unclear in our study because we did not directly compare the effects of Nox2 and Nox4 knockdown by using siRNA oligos. Our results also reveal that myoblast differentiation to myotubes coincided with a significant decline in Nox4 expression and simultaneous increase in Nox2 and $p22^{phox}$ levels (see Fig. 6). These alterations in Nox expression were associated with overall decline in O_2^- production in myotubes compared with myoblasts (see Fig. 6). We reason that this decline in O_2^- production in differentiated myotubes is a response designed to promote myogenesis because previous reports documented that oxidants inhibit myogenesis (5, 24). We should

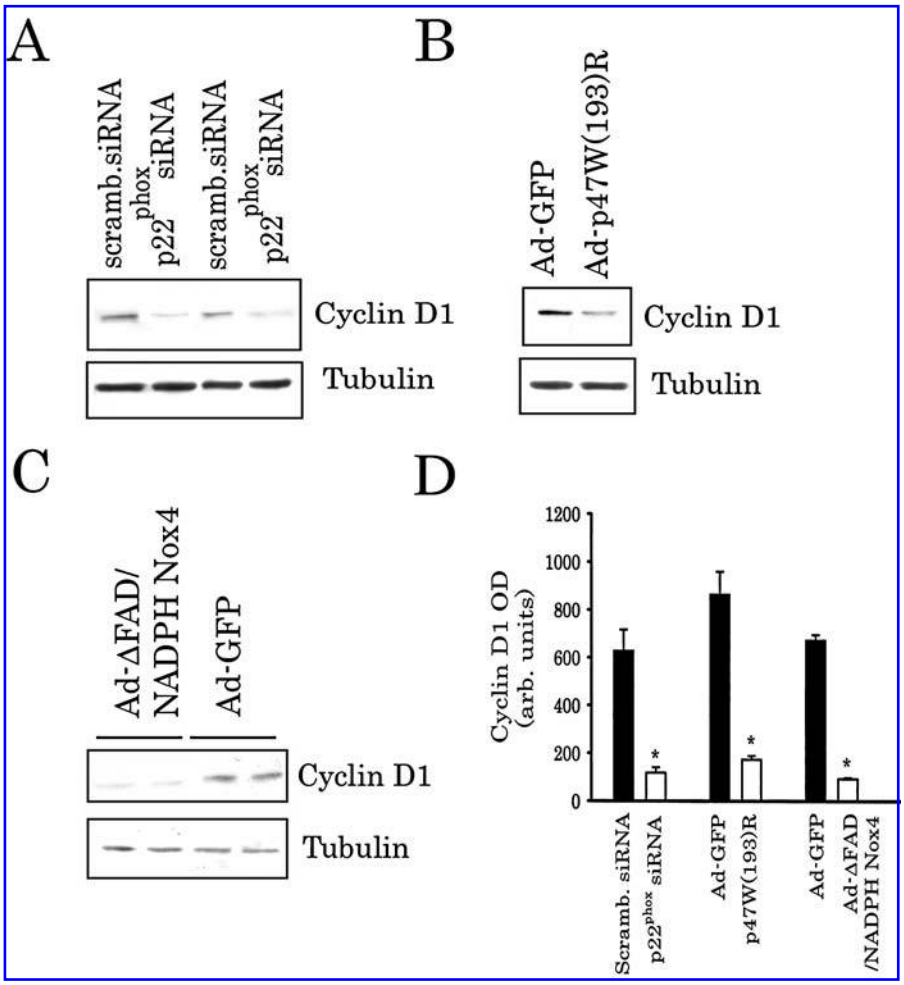

FIG. 12. Expression of cyclin D1 protein in myoblasts transfected with scrambled siRNA, $p22^{phox}$, siRNA oligonucleotides (A), myoblasts infected with adenoviruses expressing GFP or dominant-negative forms of $p47^{phox}$ (B), and Nox4 (C). (**D**) The mean values of cyclin D1 optical densities expressed in arbitrary units. $*p < 0.05$ compared with scrambled siRNA or Ad-GFP. Note that knockdown of $p22^{phox}$ or inhibition of $p47^{phox}$ and Nox4 elicits a significant decline in cyclin D1 levels.

emphasize, however, that alternative explanations exist for the reduction in O_2^- production in myotubes compared with myoblasts, other than reduction in NAPDH oxidase activity. These include alteration of cell number (because absolute O_2^- production is dependent on cell number), reduced contribution of other ROS-producing enzymes, and differences in the antioxidant levels between myotubes and myoblasts.

Regulation of myoblast proliferation by NADPH oxidase–derived ROS

It has long been established that relatively low concentrations of oxidants stimulate proliferation of mammalian cells (8). Moreover, many mitogens and growth factors acting through tyrosine kinase and G-protein–coupled receptors stimulate cell proliferation through the release of ROS, particularly from nonphagocytic NADPH oxidase (4). The present study extends these observations to skeletal muscle precursor cells and confirms that NADPH oxidase–derived ROS promote serum-induced proliferation of human skeletal precursor cells and that this effect is mediated through selective signaling pathways, including the Erk1/2, PI-3 kinase/AKT/mTOR, and the NF-κB pathways.

Many reports have confirmed that activity of the Erk1/2 pathway is redox sensitive when cells are exposed to growth factors such as PDGF, VEGF, angiotensin II, and to exogenous H_2O_2 (16, 17, 38). Likewise, our results show a strong redox-sensitive activation of the Erk1/2 pathway within 5 min of serum exposure in human skeletal myoblasts. The exact mechanisms through which the Erk1/2 pathway promotes cell proliferation are complex and include the activation of activator protein 1 (AP-1) transcription factors, which consist of homo- or heterodimers of Fos, Jun, and the ATF family of proteins. The Erk1/2 pathway promotes AP-1 activation through selective phosphorylation of c-Fos protein, which eventually leads to the entry of cells into the *S* phase (37). Our results also indicate that another member of the mitogen-activated protein kinases (MAPKs), the p38 pathway, was also activated in response to serum exposure. However, unlike the Erk1/2 protein, phosphorylation of p38 actually increased when cells were pretreated with NAC and apocynin (see Fig. 11). We propose that this increase in p38 phosphorylation might be related to the well-documented negative cross-talk between the Erk1/2 and p38 pathways, in which activation of one pathway by growth-factor receptors results in dephosphorylation and inactivation of the other pathway (18, 25, 40). It is possible; therefore, that attenuation of serum-induced Erk1/2 activation by NAC and apocynin might have also attenuated the inhibitory effect of Erk1/2 on p38 phosphorylation, resulting in further phosphorylation of the latter.

Our results also indicate that the PI-3 kinase/AKT pathway is redox sensitive in human skeletal myoblasts and that this pathway promotes serm-induced myoblast proliferation. The redox dependence of the PI-3 kinase/AKT pathway has been attributed to inactivation by ROS of the tyrosine phosphatase PTEN (31). The PI-3 kinase/AKT pathway regulates cell proliferation, in part, through the mTOR protein, which is a serine/threonine kinase that exists as two complexes, the rapamycin-sensitive mTORC1 complex and the rapamycin-insensitive mTORC2 complex (43). The PI-3 kinase/AKT pathway activates the mTOR complex by selectively inactivating the inhibitor of mTOR, resulting in enhanced mTOR phosphorylation on Ser^{2448} and an increase in mTOR activity (30, 36). Our results confirm that serum-induced phosphorylation of mTOR on Ser^{2448} is dependent on NADPH oxidase–derived ROS and that mTOR activity promotes myoblast proliferation (see Fig. 11).

In addition to the described pathways, we report here that NF-κB transcription factor is a target for NADPH oxidase-derived ROS in skeletal myoblasts. Previous studies attributed this phenomenon to the activation by ROS of upstream regulators of this pathway, the Iκ kinases (IKKα, IKKβ and IKKγ), which triggers an increase in phosphorylation and degradation of IκBα and phosphorylation and nuclear mobilization of the p65 protein (35). We confirmed that p65 phosphorylation increased significantly after 60 min of serum exposure in human skeletal myoblasts and that this phosphorylation is strongly attenuated by NAC and apocynin (see Fig. 11). Our observation that selective inhibition of NF-κB reduces myoblast proliferation suggests that NADPH oxidase–derived ROS promote proliferation of these cells, in part through the NF-κB pathway.

It should be emphasized that the targeted pathways by NADPH oxidase–derived oxidants (Erk1/2, PI-3 kinase/AKT/mTOR, and NF-κB pathways) all converge on cyclin D1 in regulating cell-cycle phases. This labile protein is required for progression through the G_1 phase in the cell cycle, and several reports have confirmed that its expression is regulated by mitogen-stimulated oxidants (6, 7). In our study, the expression of cyclin D1 was significantly reduced in human satellite cells transfected with siRNA oligos for $p22^{phox}$ and in cells infected with viruses expressing dominant-negative forms of $p47^{phox}$ and Nox4, confirming the dependence of cyclin D1 expression in these cells on NADPH oxidase–derived ROS (see Fig. 12).

In summary, our study reveals that skeletal muscle fibers and skeletal muscle precursor cells express two Nox isoforms (Nox2 and Nox4) along with $p22^{phox}$, $p67^{phox}$, and $p47^{phox}$, and that both Nox isoforms contribute to the production of O_2^- in proliferating myoblasts. Furthermore, ROS derived from NADPH oxidase activate several pathways, including the Erk1/2, PI-3 kinase/AKT, mTOR, and NF-κB pathways, resulting in significant activation of the cell-cycle machinery and increased cell proliferation.

ACKNOWLEDGMENTS

This study is supported by a grant from the Canadian Institute of Health Research and U.S. National Institute of Health grant AR42426. We are grateful to Mr. L. Franchi for his technical assistance, Dr. S. Magder for his scientific feedback, and Ms. A. Gatensby for her editorial help.

ABBREVIATIONS

AKT, protein kinase B; BrdU, bromodeoxyuridine; C_T, threshold cycle; DMEM, Dulbecco's modified Eagle's medium; DPI, diphenyleneiodonium; DTT, dithiothreitol; ECFP, enhanced cyan fluorescence protein; ECL, enhanced chemiluminescence; EDL, extensor digitorum longus; EDTA, ethylenediaminetetra acetate; ELISA, enzyme-linked immunosorbent assay; Erk1/2, extracellular regulated kinase 1 and 2; EYFP, enhanced yellow fluorescence protein; FBS, fetal bovine serum; GAPDH, glyceraldehyde phosphate dehydrogenase; GFP, green fluorescence protein; HS, horse serum; IKK, IκB kinase; mTOR, mammalian target of rapamycin; NAC, *N*-acetylcysteine; NF-κB, nuclear factor κ B; PI-3 kinase, phosphatidyl inositol 3 kinase; PMSF, phenylmethylsulfonyl fluoride; ROS, reactive oxygen species; SAPK/JNK, stress-activated protein kinase/c-Jun NH_2-terminal kinase; SiRNA, small inhibitory RNA.

REFERENCES

1. Ago T, Kitazono T, Ooboshi H, Iyama T, Han YH, Takada J, Wakisaka M, Ibayashi S, Utsumi H, and Iida M. Nox4 as the major catalytic component of an endothelial NAD(P)H oxidase. *Circulation* 109: 227–233, 2004.
2. Babior BM, Lambeth JD, and Nauseef W. The neutrophil NADPH oxidase. *Arch Biochem Biophys* 397: 342–344, 2002.
3. Banfi B, Clark RA, Steger K, and Krause KH. Two novel proteins activate superoxide generation by the NADPH oxidase NOX1. *J Biol Chem* 278: 3510–3513, 2003.
4. Bedard K and Krause KH. The NOX family of ROS-generating NADPH oxidases: physiology and pathophysiology. *Physiol Rev* 87: 245–313, 2007.
5. Buck M and Chojkier M. Muscle wasting and dedifferentiation induced by oxidative stress in a murine model of cachexia is prevented by inhibitors of nitric oxide synthesis and antioxidants. *EMBO J* 15: 1753–1765, 1996.
6. Burch PM and Heintz NH. Redox regulation of cell-cycle re-entry: cyclin D1 as a primary target for the mitogenic effects of reactive oxygen and nitrogen species. *Antioxid Redox Signal* 7: 741–751, 2005.
7. Burch PM, Yuan Z, Loonen A, and Heintz NH. An extracellular signal-regulated kinase 1- and 2-dependent program of chromatin trafficking of c-Fos and Fra-1 is required for cyclin D1 expression during cell cycle reentry. *Mol Cell Biol* 24: 4696–4709, 2004.
8. Burdon RH. Superoxide and hydrogen peroxide in relation to mammalian cell proliferation. *Free Radic Biol Med* 18: 775–794, 1995.
9. Cai H, Griendling KK, and Harrison DG. The vascular NAD(P)H oxidases as therapeutic targets in cardiovascular diseases. *Trends Pharmacol Sci* 24: 471–478, 2003.
10. Cheng G, Cao Z, Xu X, van Meir EG, and Lambeth JD. Homologs of $gp91^{phox}$: cloning and tissue expression of Nox3, Nox4, and Nox5. *Gene* 269: 131–140, 2001.
11. Deveci D, Marshall JM, and Egginton S. Relationship between capillary angiogenesis, fiber type, and fiber size in chronic systemic hypoxia. *Am J Physiol Heart Circ Physiol* 281: H241–H252, 2001.
12. Espinosa A, Leiva A, Pena M, Muller M, Debandi A, Hidalgo C, Carrasco MA, and Jaimovich E. Myotube depolarization generates reactive oxygen species through NAD(P)H oxidase; ROS-elicited Ca^{2+} stimulates ERK, CREB, early genes. *J Cell Physiol* 209: 379–388, 2006.
13. Goyal P, Weissmann N, Rose F, Grimminger F, Schafers HJ, Seeger W, and Hanze J. Identification of novel Nox4 splice variants with impact on ROS levels in A549 cells 2. *Biochem Biophys Res Commun* 329: 32–39, 2005.
14. Gu Y, Xu YC, Wu RF, Nwariaku FE, Souza RF, Flores SC, and Terada LS. $p47^{phox}$ participates in activation of RelA in endothelial cells. *J Biol Chem* 278: 17210–17217, 2003.

15. Gu Y, Xu YC, Wu RF, Souza RF, Nwariaku FE, and Terada LS. TNFα activates c-Jun amino terminal kinase through p47(phox). *Exp Cell Res* 272: 62–74, 2002.
16. Gupta K, Kshirsagar S, Li W, Ramakrishnam S, Gui L, Gupta P, Law PY, and Hebbel RP. VEGF prevents apoptosis of human microvascular endothelial cells via opposing effects on MAPK/ERK and SAPK/JNK signaling. *Exp Cell Res* 247: 495–504, 1999.
17. Guyton KZ, Liu Y, Gorospe M, Xu Q, and Holbrook NJ. Activation of mitogen-activated protein kinase by H_2O_2: role in cell survival following oxidant injury. *J Biol Chem* 271: 4138–4142, 1996.
18. Harfouche R, Gratton JP, Yancopoulos GD, and Hussain SNA. Angiopoietin-1 activates both anti- and pro-apoptotic mitogen activated protein kinases. *FASEB J* 17: 1523–1525, 2003.
19. Hawke TJ and Garry DJ. Myogenic satellite cells: physiology to molecular biology. *J Appl Physiol* 91: 534–551, 2001.
20. Hidalgo C, Sanchez G, Barrientos G, and Racena-Parks P. A transverse tubule NADPH oxidase activity stimulates calcium release from isolated triads via ryanodine receptor type 1 S -glutathionylation. *J Biol Chem* 281: 26473–26482, 2006.
21. Hutchinson DS, Csikasz RI, Yamamoto DL, Shabalina IG, Wikström P, Wilcke M, and Bengtsson T. Diphenylene iodonium stimulates glucose uptake in skeletal muscle cells through mitochondrial complex I inhibition and activation of AMP-activated protein kinase. *Cell Signal* 19: 1610–1620, 2007.
22. Javeshghani D, Magder S, Barreiro E, Quinn MT, and Hussain SNA. Molecular characterization of a superoxide-generating NAD(P)H oxidase in the ventilatory muscles. *Am J Resp Crit Care Med* 165: 412–418, 2002.
23. Lambeth JD. NOX enzymes and the biology of reactive oxygen. *Nat Rev Immunol* 4: 181–189, 2004.
24. Langen RC, Schols AM, Kelders MC, van d, V, Wouters EF, and Janssen-Heininger YM. Tumor necrosis factor-α inhibits myogenesis through redox-dependent and -independent pathways. *Am J Physiol Cell Physiol* 283: C714–C721, 2002.
25. Li SP, Junttila MR, Han J, Kahari VM, and Westermarck J. p38 Mitogen-activated protein kinase pathway suppresses cell survival by inducing dephosphorylation of mitogen-activated protein/extracellular signal-regulated kinase kinase1,2. *Cancer Res* 63: 3473–3477, 2003.
26. Li Y, Zhu H, Kuppusamy P, Roubaud V, Zweier JL, and Trush MA. Validation of lucigenin (bis-N-methylacridinium) as a chemiluminescence probe for detecting superoxide anions radical production by enzymatic and cellular systems. *J Biol Chem* 273: 2015–2023, 1998.
27. Liochev SI and Fridovich I. Lucigenin (bis-N-methylacridinium) as a mediator of superoxide anion production. *Arch Biochem Biophys* 337: 115–120, 1997.
28. Lochmuller H, Johns T, and Shoubridge EA. Expression of the E6 and E7 genes of human papillomavirus (HPV16) extends the life span of human myoblasts. *Exp Cell Res* 248: 186–193, 1999.
29. Mahadev K, Zilbering A, Zhu L, and Goldstein BJ. Insulin-stimulated hydrogen peroxide reversibly inhibits protein-tyrosine phosphatase 1b in vivo and enhances the early insulin action cascade. *J Biol Chem* 276: 21938–21942, 2001.
30. Manning BD, Logsdon MN, Lipovsky AI, Abbott D, Kwiatkowski DJ, and Cantley LC. Feedback inhibition of Akt signaling limits the growth of tumors lacking Tsc2. *Genes Dev* 19: 1773–1778, 2005.
31. Meng TC, Fukada T, and Tonks NK. Reversible oxidation and inactivation of protein tyrosine phosphatases in vivo. *Mol Cell* 9: 387–399, 2002.
32. Petry A, Djordjevic T, Weitnauer M, Kietzmann T, Hess J, and Gorlach A. NOX2 and NOX4 mediate proliferative response in endothelial cells. *Antioxid Redox Signal* 8: 1473–1484, 2006.
33. Rosenblatt JD, Lunt AI, Parry DJ, and Partridge TA. Culturing satellite cells from living single muscle fiber explants. *In Vitro Cell Dev Biol Anim* 31: 773–779, 1995.
34. Sanlioglu S, Williams CM, Samavati L, Butler NS, Wang G, McCray PB Jr, Ritchie TC, Hunninghake GW, Zandi E, and Engelhardt JF. Lipopolysaccharide induces Rac1-dependent reactive oxygen species formation and coordinates tumor necrosis factor-alpha secretion through IKK regulation of NF-κB. *J Biol Chem* 276: 30188–30198, 2001.
35. Schreck R, Rieber P, and Baeuerle PA. Reactive oxygen intermediates as apparently widely used messengers in the activation of the NF-κB transcription factor and HIV-1. *EMBO J* 10: 2247–2258, 1991.
36. Sekulic A, Hudson CC, Homme JL, Yin P, Otterness DM, Karnitz LM, and Abraham RT. A direct linkage between the phosphoinositide 3-kinase-AKT signaling pathway and the mammalian target of rapamycin in mitogen-stimulated and transformed cells. *Cancer Res* 60: 3504–3513, 2000.
37. Shaulian E and Karin M. AP-1 in cell proliferation and survival. *Oncogene* 20: 2390–2400, 2001.
38. Sundaresan M, Yu ZX, Ferrans VJ, Irani K and Finkel T. Requirement for generation of H_2O_2 for platelet-derived growth factor signal transduction. *Science* 270: 296–299, 1995.
39. Toniolo L, Maccatrozzo L, Patruno M, Caliaro F, Mascarello F, and Reggiani C. Expression of eight distinct MHC isoforms in bovine striated muscles: evidence for MHC-2B presence only in extraocular muscles. *J Exp Biol* 208: 4243–4253, 2005.
40. Wang Z, Yang H, Tachado SD, Capo-Aponte JE, Bildin VN, Koziel H, and Reinach PS. Phosphatase-mediated crosstalk control of ERK and p38 MAPK signaling in corneal epithelial cells. *Invest Ophthalmol Vis Sci* 47: 5267–5275, 2006.
41. Wei Y, Sowers JR, Nistala R, Gong H, Uptergrove GM, Clark SE, Morris EM, Szary N, Manrique C, and Stump CS. Angiotensin II-induced NADPH oxidase activation impairs insulin signaling in skeletal muscle cells. *J Biol Chem* 281: 35137–35146, 2006.
42. Wu RF, Gu Y, Xu YC, Nwariaku FE, and Terada LS. Vascular endothelial growth factor causes translocation of $p47^{phox}$ to membrane ruffles through WAVE1. *J Biol Chem* 278: 36830–36840, 2003.
43. Wullschleger S, Loewith R, and Hall MN. TOR signaling in growth and metabolism. *Cell* 124: 471–484, 2006.

Address reprint requests to:
Dr. S. Hussain
Room L305,
687 Pine Ave West
Royal Victoria Hospital
Montréal, Québec H3A 1A1
Canada

E-mail: sabah.hussain@muhc.mcgill.ca

Date of first submission to ARS Central, June 18, 2007; date of final revised submission, September 24, 2007; date of acceptance, September 29, 2007.

This article has been cited by:

1. Marina Sciancalepore, Elisa Luin, Giulia Parato, Elisa Ren, Rashid Giniatullin, Elsa Fabbretti, Paola Lorenzon. 2012. Reactive oxygen species contribute to the promotion of the ATP-mediated proliferation of mouse skeletal myoblasts. *Free Radical Biology and Medicine* **53**:7, 1392-1398. [CrossRef]
2. Eberhard Schulz , Philip Wenzel , Thomas Münzel , Andreas Daiber . Mitochondrial Redox Signaling: Interaction of Mitochondrial Reactive Oxygen Species with Other Sources of Oxidative Stress. *Antioxidants & Redox Signaling*, ahead of print. [Abstract] [Full Text HTML] [Full Text PDF] [Full Text PDF with Links]
3. Jinah Choi. 2012. Oxidative stress, endogenous antioxidants, alcohol, and hepatitis C: Pathogenic interactions and therapeutic considerations. *Free Radical Biology and Medicine* . [CrossRef]
4. Karen A. M. Kennedy, Shelley D. E. Sandiford, Ilona S. Skerjanc, Shawn S.-C. Li. 2011. Reactive oxygen species and the neuronal fate. *Cellular and Molecular Life Sciences* . [CrossRef]
5. Gayle Gordillo , Huiqing Fang , Hana Park , Sashwati Roy . 2010. Nox-4–Dependent Nuclear H2O2 Drives DNA Oxidation Resulting in 8-OHdG as Urinary Biomarker and Hemangioendothelioma Formation. *Antioxidants & Redox Signaling* **12**:8, 933-943. [Abstract] [Full Text HTML] [Full Text PDF] [Full Text PDF with Links] [Supplemental material]
6. Barbara Lener, Rafa# Kozie#, Haymo Pircher, Eveline Hütter, Ruth Greussing, Dietmar Herndler#Brandstetter, Martin Hermann, Hermann Unterluggauer, Pidder Jansen#Dürr. 2009. The NADPH oxidase Nox4 restricts the replicative lifespan of human endothelial cells. *Biochemical Journal* **423**:3, 363-374. [CrossRef]
7. Célio X.C. Santos , Leonardo Y. Tanaka , João Wosniak , Jr. , Francisco R.M. Laurindo . 2009. Mechanisms and Implications of Reactive Oxygen Species Generation During the Unfolded Protein Response: Roles of Endoplasmic Reticulum Oxidoreductases, Mitochondrial Electron Transport, and NADPH Oxidase. *Antioxidants & Redox Signaling* **11**:10, 2409-2427. [Abstract] [Full Text HTML] [Full Text PDF] [Full Text PDF with Links] [Supplemental material]
8. Masuko Ushio-Fukai , Norifumi Urao . 2009. Novel Role of NADPH Oxidase in Angiogenesis and Stem/Progenitor Cell Function. *Antioxidants & Redox Signaling* **11**:10, 2517-2533. [Abstract] [Full Text HTML] [Full Text PDF] [Full Text PDF with Links]
9. Elsa C. Chan, Fan Jiang, Hitesh M. Peshavariya, Gregory J. Dusting. 2009. Regulation of cell proliferation by NADPH oxidase-mediated signaling: Potential roles in tissue repair, regenerative medicine and tissue engineering. *Pharmacology & Therapeutics* **122**:2, 97-108. [CrossRef]
10. Narasimman Gurusamy , Subhendu Mukherjee , Istvan Lekli , Claudia Bearzi , Silvana Bardelli , Dipak K. Das . 2009. Inhibition of Ref-1 Stimulates the Production of Reactive Oxygen Species and Induces Differentiation in Adult Cardiac Stem Cells. *Antioxidants & Redox Signaling* **11**:3, 589-599. [Abstract] [Full Text HTML] [Full Text PDF] [Full Text PDF with Links]
11. J. David Lambeth, Karl-Heinz Krause, Robert A. Clark. 2008. NOX enzymes as novel targets for drug development. *Seminars in Immunopathology* **30**:3, 339-363. [CrossRef]